STAR FORMATION NEWSLETTER #302 6 - 13

泉奈都子 (NAOJ)

Paper list

6. **Sulphur monoxide exposes a potential molecular disk wind from the planet-hosting disk around HD 100546**
   Alice S. Booth et al.
7. **The lithium-rotation connection in the 125 Myr-old Pleiades cluster**
   J. Bouvier et al.
8. **The dense cores and filamentary structure of the molecular cloud in Corona Australis. Herschel SPIRE and PACS observations from the Herschel Gold Belt Survey**
   D. Bresnahan et al.
9. **(The) Radio outburst from a massive (proto)star: When accretion turns into ejection**
   R. Casaroni et al.
10. **Binary energy source of the HH 250 outflow and its circumstellar environment**
    F. Comeron et al.
11. **The ionizing source of the bipolar HII region S106: a close massive binary**
    F. Comeron et al.
12. **The embedded ring-like feature and star formation activities in G35.673-00.847**
    Lokesh K. Dewangan et al.
13. **Rings and gaps in the disk around Elias 24 revealed by ALMA**
    G. Dipierro et al.

6. Sulphur monoxide exposes a potential molecular disk wind from the planet-hosting disk around HD 100546

Alice S. Booth et al. Accepted by A&A https://arxiv.org/pdf/1712.05992

Planet-hosting diskにおけるSOの観測

- **HD 100546**
  - Herbig Be star
  - 2.4 $M_\odot$
  - ~ 109 pc
  - Position angle: 146°, inclination: 44°
  - 2つの惑星が検出（20M_J at 10au, 15M_J at 68 au）

- **Observation**
  - ALMA Band7
  - 4 SO transition

- **Results**
  - SO 7_7-6_6, 7_8-6_7 を検出

Table 1: ALMA band 7 observational parameters and sulphur monoxide transitions for HD 100546

Date observed	18th November 2012				
Baselines	21 - 375 m				
Weighting	natural				
SO rotational transitions	7_7-6_6	7_8-6_7	8_8-7_7	3_2-1_2	$7_7-6_6+7_8-6_7$
Rest frequency (GHz)	301.286	304.078	344.311	345.704	-
Synthesised beam	1.″1 × 0.″6	1.″1 × 0.″6	1.″0 × 0.″5	1.″0 × 0.″5	1.″1 × 0.″6
Beam P.A.	24°	23°	40°	40°	24°
Spectral resolution (km s^{-1})	0.24	0.24	0.21	0.21	1.00
r.m.s noise (channel^{-1} mJy $beam^{-1}$)	10.9	9.9	17.4	16.2	4.2
Peak emission (mJy $beam^{-1}$)	-	-	-	-	24.7
E_u (K)	71.0	62.1	87.5	21.1	-
Einstein A coefficient (s^{-1})	3.429e-04	3.609e-04	5.186e-04	1.390e-07	-

The values for the line frequencies and Einstein A coefficients are from the Cologne Database for Molecular Spectroscopy (CDMS; Müller et al. 2001) and the Leiden Atomic and Molecular Database (LAMDA; Schöier et al. 2005).

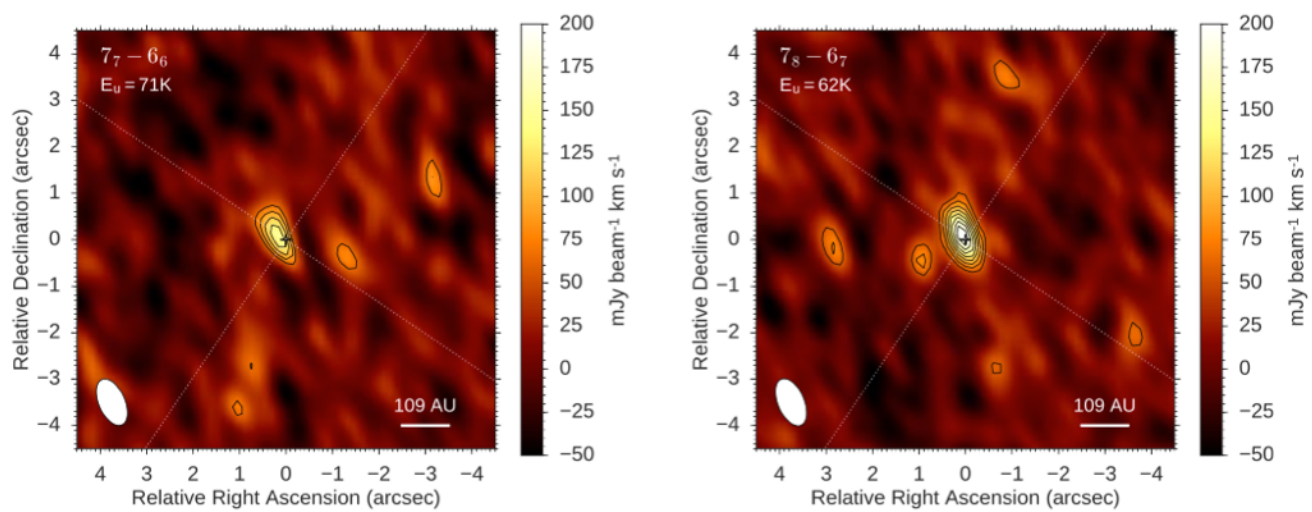

Fig. 1: Integrated intensity maps of the two SO transitions taken over a 11 km s^{-1} velocity range. Left: the J = 7_7-6_6 transition with an r.m.s of 22 mJy $beam^{-1}$ km s^{-1} and a peak emission of 151 mJy $beam^{-1}$ km s^{-1} resulting in a S/N of 6.9. Right: the J = 7_8-6_7 transition with an r.m.s of 19 mJy $beam^{-1}$ km s^{-1} and a peak emission of 206 mJy $beam^{-1}$ km s^{-1} resulting in a S/N of 10.8. The black contours are at intervals of σ going from 3σ to peak.

- **Results**
  - 2つの速度構造を持つ（source, Blue-shift）
  - SOの分布はCOよりcompact
  - source部分のSOはminor axisに対して非対称であり、北東にピークあり
  - Blue-shift側のSOの分布はCOと合わない
  - Kinematics, spatial distributionはKeplerian diskと合わない
  - Blue-shift は Disk wind 成分を示すだろう

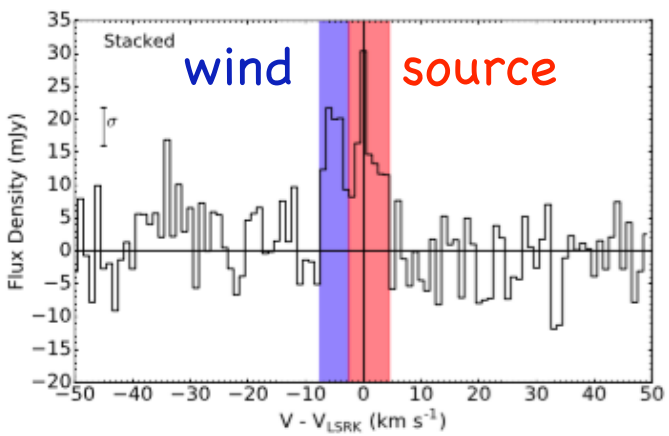

Fig. 3: Line profile extracted from within the 3σ extent of the SO stacked integrated intensity with an r.m.s. noise of 5.7 mJy and a peak flux of 30.4 mJy resulting in a S/N of 5.3. Highlighted in red and blue are the velocity ranges of emission used in the moment maps of the individual lines in Figure 4.

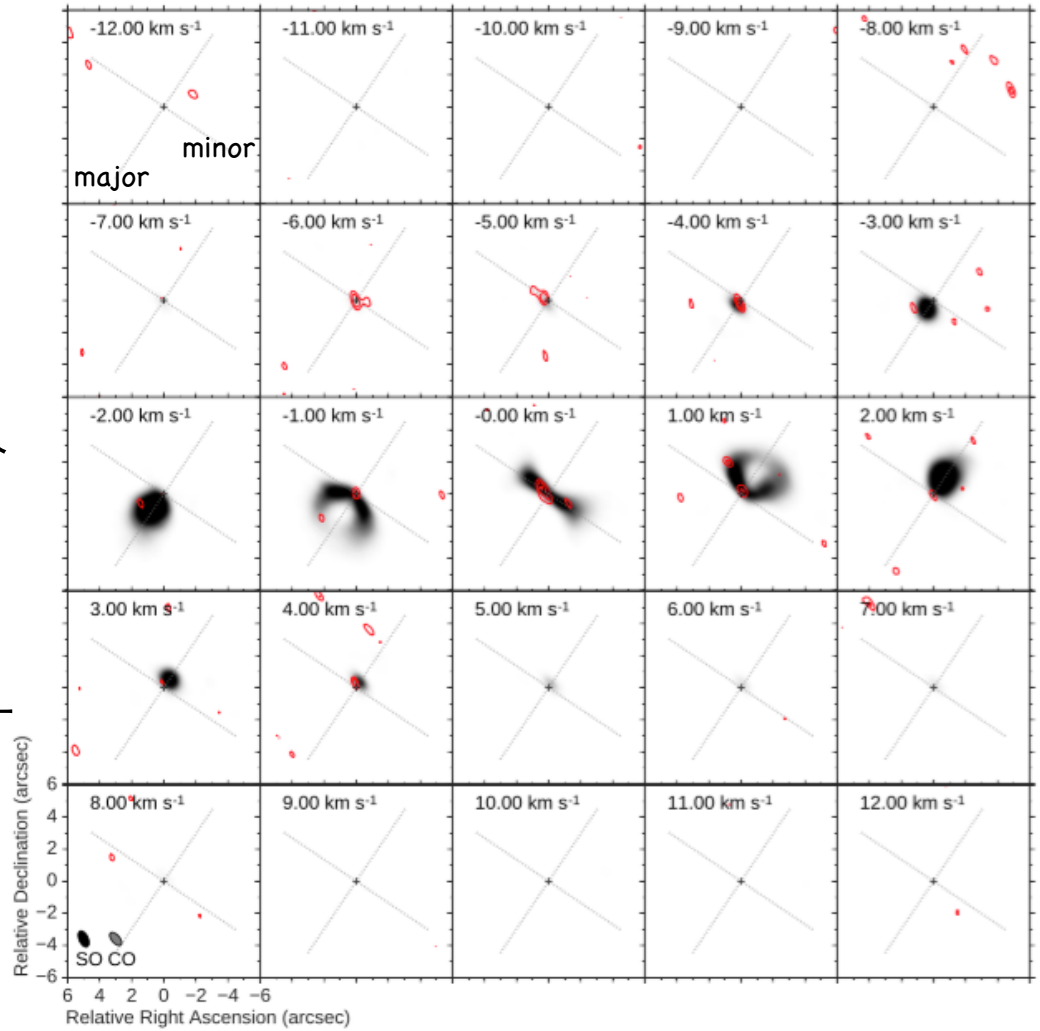

Fig. 2: Channel maps of the stacked SO emission (red contours) and the CO J = 3 – 2 emission with a 3σ clip (grey colour map). The stacked SO emission has with an r.m.s. noise of 4.2 mJy beam^{-1} channel^{-1} and peak emission of 24.7 mJy beam^{-1} resulting in a peak S/N of 5.9. The contours are from 3σ to peak in intervals of σ. The velocities stated are with respect to the source velocity of the emission.

- **Results**
  - SOはdisk内部の20-100 auの領域に分布
  - Diskの北東部分は中心星から温められ、disk windが吹く状況を作り出している?

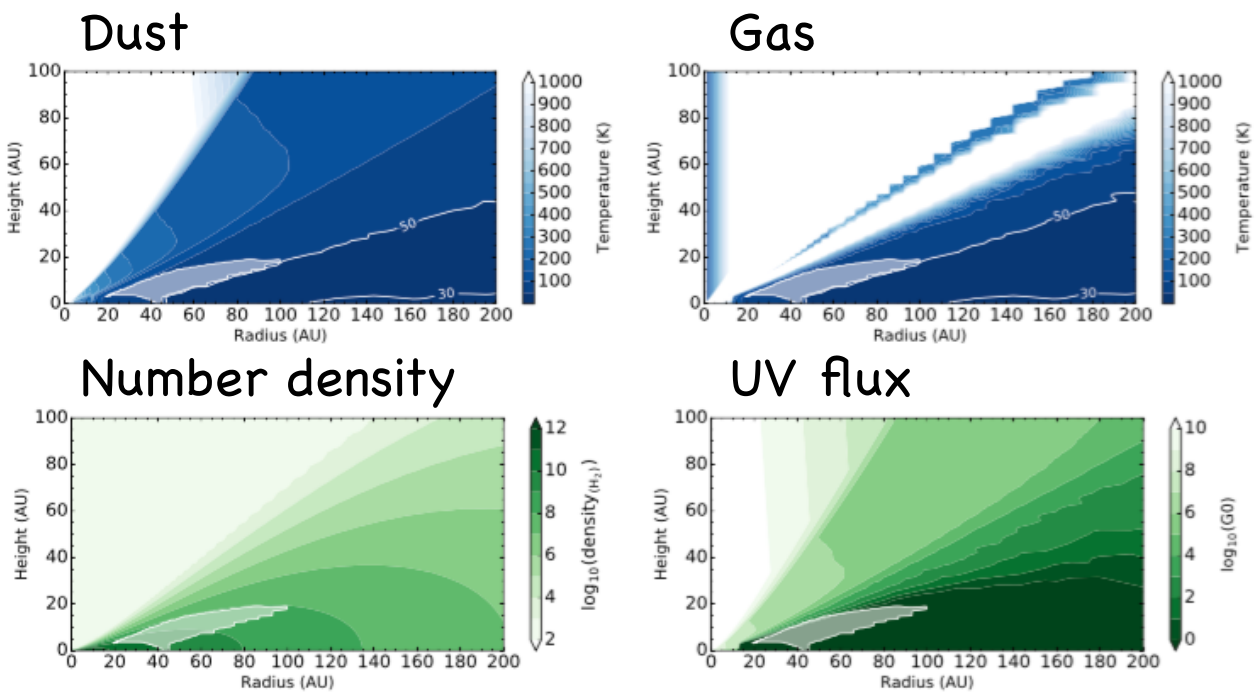

Fig. 6: The HD 100546 disk physical structure from Kama et al. (2016). Top left and moving clockwise: the dust temperature (K), gas temperature (K), UV flux (in units of the interstellar radiation field) and number density (cm^{-3}). The two white contours in each of the temperature plots correspond to temperatures 30 K and 50 K. The shaded region highlights the location of the SO motivated by RADEX calculations and used in the LIME modelling.

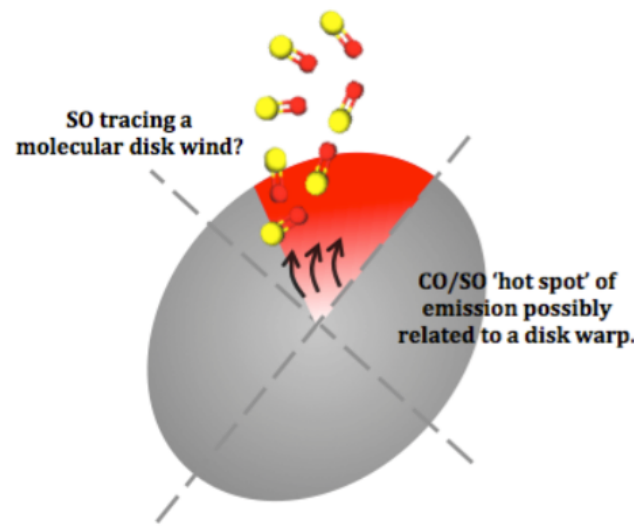

Fig. 9: Cartoon of HD 100546 wedge disk emission and SO disk wind.

9. Radio outburst from a massive (proto) star: When accretion turns into ejection

R. Casaroni et al. Accepted by A&A https://arxiv.org/pdf/1802.04228.pdf

YSOのaccretion, ejection現象の関係:密接に関連している (accretion => jet)と予想
=> Radio emissionの増加現象（jet）が IRの増加現象（accretion）の後に見られる?

- **S255 NIRS 3**
  - Accretion の結果、methanol maserとIR emissionにおける増加が見られた天体
- **Observation**
  - VLA
    - 6.0, 10.0, 22.2, 45.5 GHz
  - IRAM/NOEMA
    - 3.6, 87, 150 GHz
  - ALMA
    - 85.2, 87.2, 97.2, 99.2 GHz
- **Result**

Table 1. Flux densities measured towards the central core of S255 NIRS 3 with the VLA, IRAM/NOEMA, and ALMA at different epochs, and corresponding mean synthesized beams. Months from March to December refer to 2016, while January and February refer to 2017.

date	Mar	Jul	Aug	Oct	Nov	Dec	Jan	Feb
ν				S_ν, HPBW				
(GHz)	(mJy, arcsec)	(mJy, arcsec)	(mJy, arcsec)	(mJy, arcsec)	(mJy, arcsec)	(mJy, arcsec)	(mJy, arcsec)	(mJy, arcsec)
6	0.87, 2.54	0.79, 0.998	1.1, 1.33	2.6, 0.358	4.8, 0.402	7.9, 0.352	–	–
10	1.0, 1.64	1.2, 0.609	1.8, 0.765	3.6, 0.168	6.7, 0.235	11, 0.209	–	–
22.2	2.7, 0.73	2.2, 0.354	3.1, 0.351	6.6, 0.0695	11, 0.108	18, 0.0969	–	–
45.5	4.4, 0.412	1.9, 0.190	3.8, 0.195	14, 0.0437	21, 0.0455	27, 0.0800	–	–
86.2	–	–	–	–	–	73, 2.5	–	–
87	–	–	–	–	–	–	57, 4.2	64, 4.1
98.2	–	–	–	–	–	90, 2.2	–	–
150	–	–	–	–	–	–	175, 2.4	168, 2.3

Moscadelli et al. 2017 Fig1

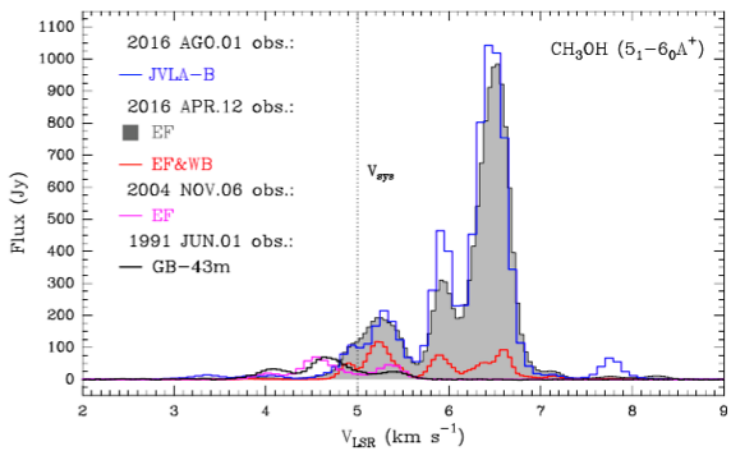

Fig. 1. Comparison of 6.7 GHz CH_3OH maser spectra obtained toward NIRS 3. Two single-dish pre-burst spectra obtained with the Green Bank (GB–43 m, black) and Effelsberg (EF, magenta) antennas are compared with the emission detected during the outburst phase at three different baselines: an EF total-power (filled histogram), a cross-power (red) of the EF and Westerbork (WB) baseline (~250 km), and a synthesized VLA spectrum (blue) obtained in the B configuration (maximum baseline of 11 km). The legend on the left side reports the observing dates. The dotted vertical line indicates the systemic velocity (V_{sys}) of the source S255-SMA1 from Zinchenko et al. (2015).

- **Results**
  - Radio emissionにおける増加傾向を検出（IR の増加に伴うものとしては**初**検出）

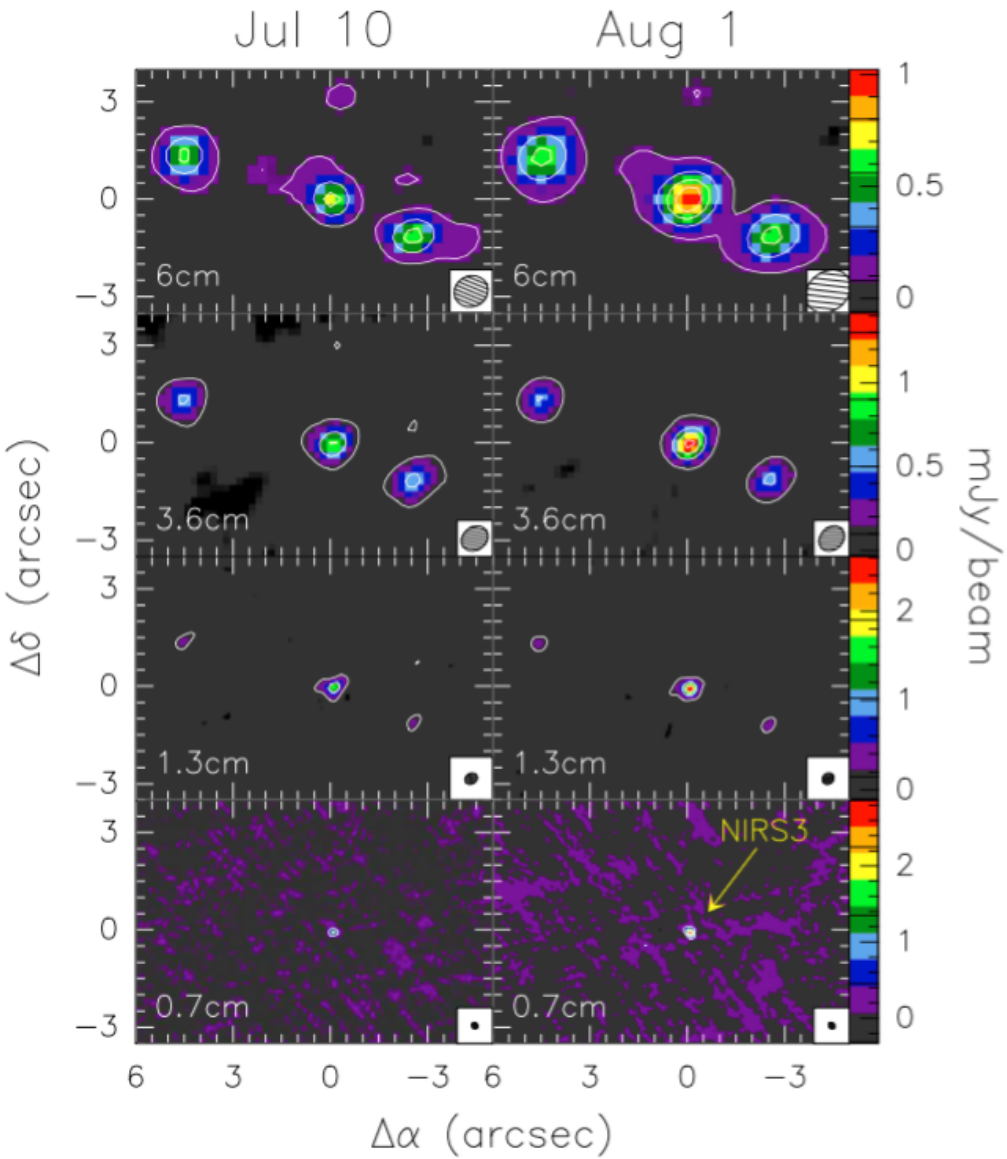

Fig. 2. Maps of the S255 NIRS 3 region at centimetre wavelengths obtained with the VLA on July 10 (left panels) and August 1 (right panels), 2016. The offsets are computed with respect to the phase centre of the observations, i.e. $06^h\,12^m\,54\overset{s}{.}02$, $17^\circ\,59'\,23\overset{''}{.}1$. The corresponding synthesized beams are shown at the bottom right of each panel. The values of the contour levels are marked in the colour scales to the right, and in all cases the lowest contour is $> 4\sigma$. We note the brightening of NIRS 3 at all frequencies.

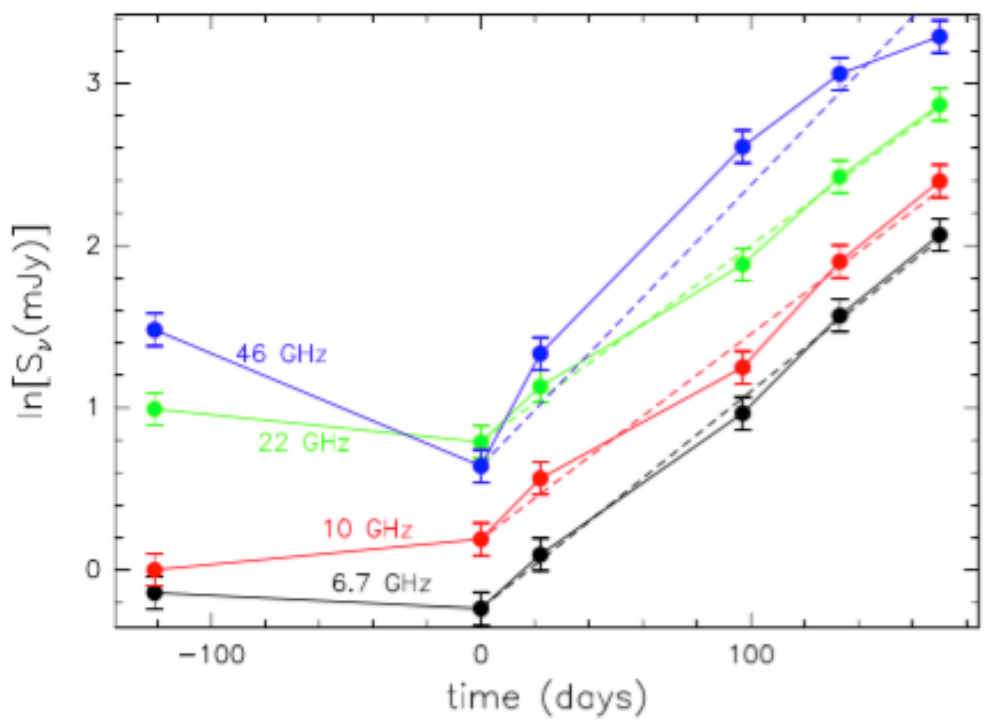

Fig. 3. Observed radio flux densities of NIRS 3 as a function of time, with t=0 corresponding to the second epoch of our monitoring (July 10, 2016). The solid lines connect fluxes observed at the same frequency, which is given beside each curve. The dashed lines are the fits assuming exponential dependence on t according to Eq. (1).

12. The embedded ring-like feature and star formation activities in G35.673-00.847

L. K. Dewangan et al. Accepted by ApJ http://xxx.lanl.gov/pdf/1801.07364v1

HII regionに付随しないstellar cluster/ring-like featureの形成について (磁場の影響)

- **G35.673-00.847**
  - 距離: 3.7 kpc
  - HII regionの存在が確認
    - その近くにsemi-ring-like 構造が見られている
- **Multi-wavelength data**

Table 1
List of surveys (covering from NIR to radio wavelengths) adopted in this work.

Survey	Wavelength(s)	Resolution ($''$)	Reference
Two Micron All Sky Survey (2MASS)	1.25–2.2 μm	∼2.5	Skrutskie et al. (2006)
Galactic Plane Infrared Polarization Survey (GPIPS)	1.6 μm	∼1.5	Clemens et al. (2012a)
UKIRT NIR Galactic Plane Survey (GPS)	1.25–2.2 μm	∼0.8	Lawrence et al. (2007)
Spitzer Galactic Legacy Infrared Mid-Plane Survey Extraordinaire (GLIMPSE)	3.6, 4.5, 5.8, 8.0 μm	∼2, ∼2, ∼2, ∼2	Benjamin et al. (2003)
Wide Field Infrared Survey Explorer (WISE)	3.4, 4.6, 12, 22 μm	∼6, ∼6.5, ∼6.5, ∼12	Wright et al. (2010)
Spitzer MIPS Inner Galactic Plane Survey (MIPSGAL)	24 μm	∼6	Carey et al. (2005)
Herschel Infrared Galactic Plane Survey (Hi-GAL)	70, 160, 250, 350, 500 μm	∼5.8, ∼12, ∼18, ∼25, ∼37	Molinari et al. (2010)
Planck polarization data	850 μm	∼294	Planck Collaboration IX (2014)
Galactic Ring Survey (GRS)	2.7 mm; ^{13}CO (J = 1–0)	∼45	Jackson et al. (2006)
Coordinated Radio and Infrared Survey for High-Mass Star Formation (CORNISH)	6 cm	∼1.5	Hoare et al. (2012)
NRAO VLA Sky Survey (NVSS)	21 cm	∼45	Condon et al. (1998)

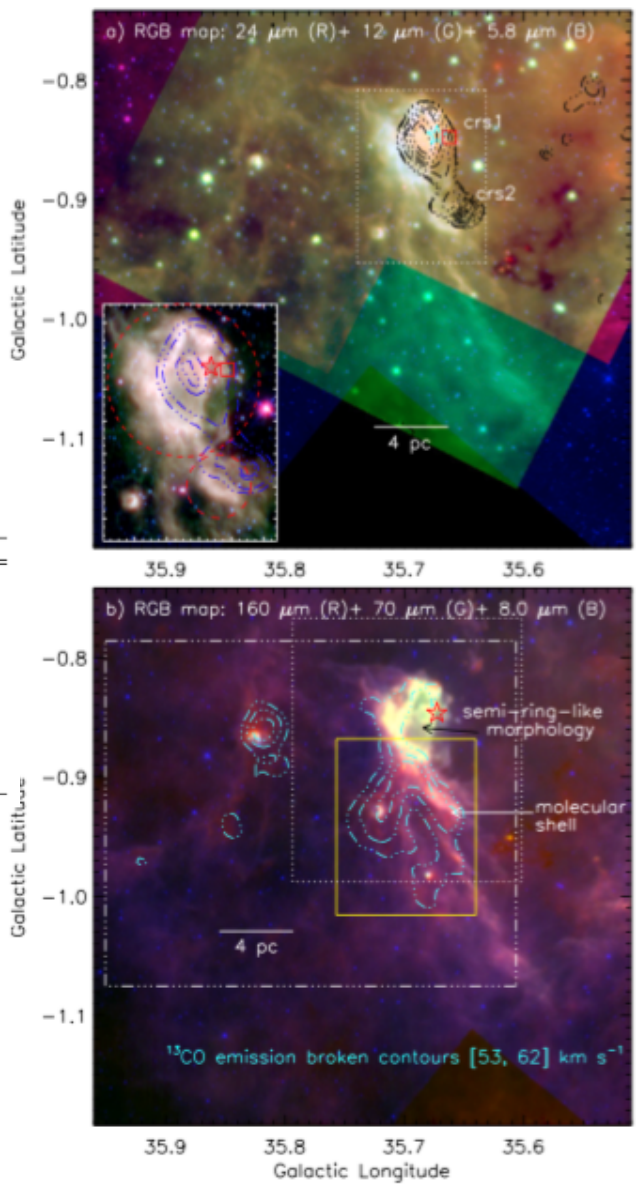

Figure 1. A large-scale view of the G35.6 site (size of the selected field ∼27′ × 27′; central coordinates: $l = 35^{\circ}.735$; $b = -0^{\circ}.967$). a) The image is the result of the combination of three bands (in log scale): 24.0 μm in red (*Spitzer*), 12.0 μm in green (*WISE*), and 5.8 μm in blue (*Spitzer*). Contours of NVSS 1.4 GHz radio continuum emission (beam size ∼45″) are superimposed with 8, 10, 20, 30, 40, 55, 70, 85, and 95% of the peak value (i.e., 31.7 mJy/beam). Two compact radio sources (i.e., crs1 and crs2) traced in the NVSS 1.4 GHz map are highlighted in the figure. The inset on the bottom left shows the H II regions in zoomed-in view, using a color-composite image (*WISE* 12.0 μm (in red), *Spitzer* 8.0 μm (in green), and *Spitzer* 5.8 μm (in blue)) overlaid with the NVSS radio continuum emission at 1.4 GHz (see a dashed white box in figure). In the inset, the NVSS contours are 2.5, 6, 20, and 25 mJy/beam. A red square indicates the position of a CORNISH 5 GHz radio source, G035.6624-00.8481 (see also the inset). b) The image is the result of the combination of three bands: *Herschel* 160 μm (red), *Herschel* 70 μm (green), and *Spitzer* 8.0 μm (blue). The composite map is also overlaid with the ^{13}CO emission contours integrated over a velocity interval from 53 to 62 km s^{-1}. The ^{13}CO contours are shown with the levels of 4.5, 8, and 12 K km s^{-1}. A small dotted box (in white) shows the area investigated by Paron et al. (2011). A semi-ring-like morphology and a molecular shell are also highlighted in the figure (see also Paron et al. 2011). A solid box (in yellow) encompasses the area shown in Figure 2. A big dotted-dashed box (in white) encompasses the area shown in Figures 3 and 4a. In all the panels, a star symbol indicates the position of IRAS 18569+0159. The scale bar corresponding to 4 pc (at a distance of 3.7 kpc) is shown in both the panels.

- **Results**
  - Embedded face-on ring-like featureを検出(1.4 GHzのradio continuumでは見検出)
    - 大質量星のfeed-backによるものではない
    - Hershel clump, YSOがが内部に検出

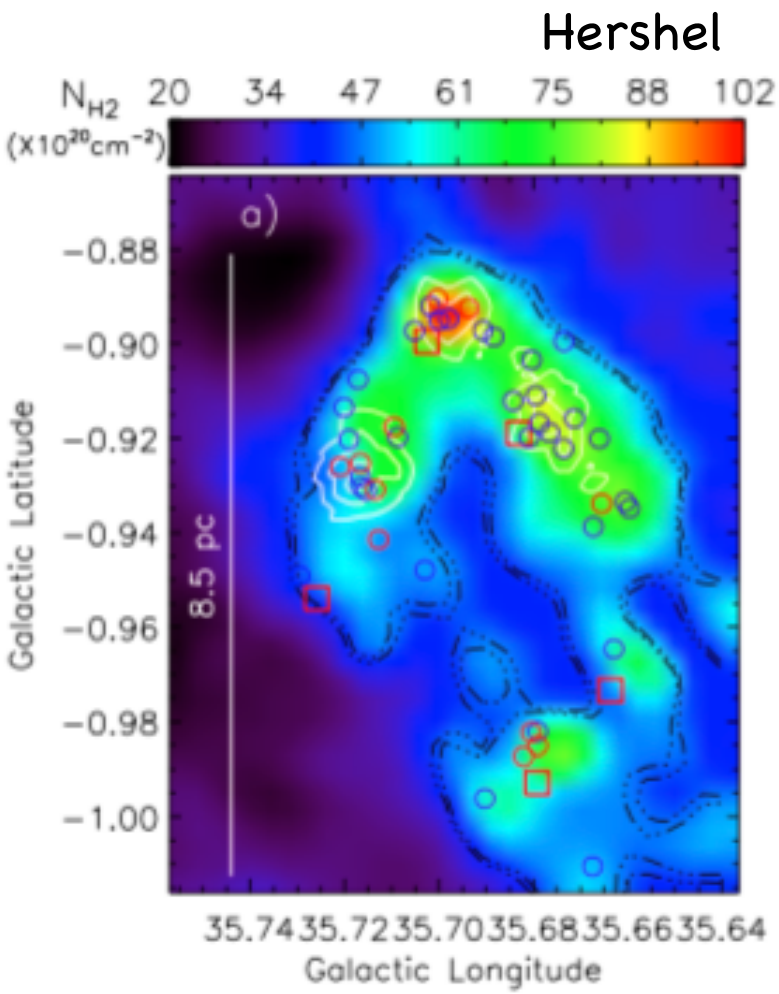

Figure 12. Zoomed-in view of the ring-like feature. a) *Herschel* column density map is superimposed with surface density contours (in white) of all the identified YSOs, *Herschel* clumps and selected YSOs. b) Overlay of GPIPS H-band polarization vectors (in red) of high quality background

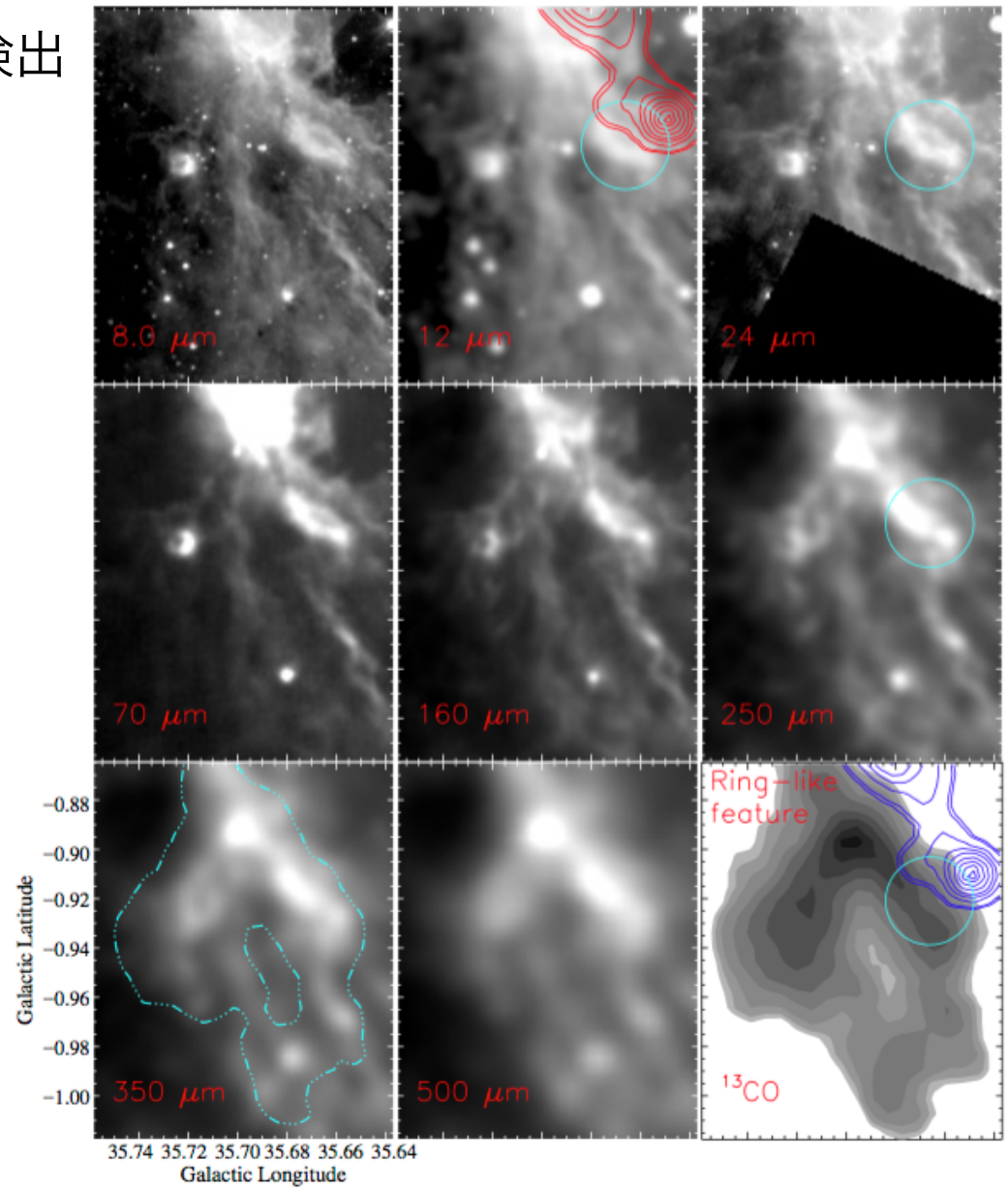

Figure 2. A zoomed-in multi-wavelength view of a ring-like feature. The panels present images at 8.0 μm, 12 μm, 24 μm, 70 μm, 160 μm, 250 μm, 350 μm, and 500 μm, and integrated ^{13}CO contour map, from the GLIMPSE, WISE, MIPSGAL, Hi-GAL, and GRS surveys (from left to right in increasing order). The integrated ^{13}CO contour map is similar to the one shown in Figure 5a. The integrated ^{13}CO contour map and the image at 12 μm are overlaid with the NVSS 1.4 GHz continuum emission contours, which are similar to the one shown in Figure 1a. A ^{13}CO contour is superimposed on the 350 μm map with a level of 3.8 K km s^{-1}. The ring-like feature is prominently evident at wavelengths longer than 160 μm, and does not contain ionized gas emission at its interior. A small feature seen in the infrared and sub-mm images is also highlighted by a circle in four panels.

- **Results**
  - 磁場はring-like featureの長軸方向に平行
  - Ring-like featureの中の3つのclumpはmagnetically supercritical (乱流>磁場, 活発に星生成が起こる=>星団形成)
    => Li & Nakamuraの理論（subcritical cloudsのfragmentation）で説明可能

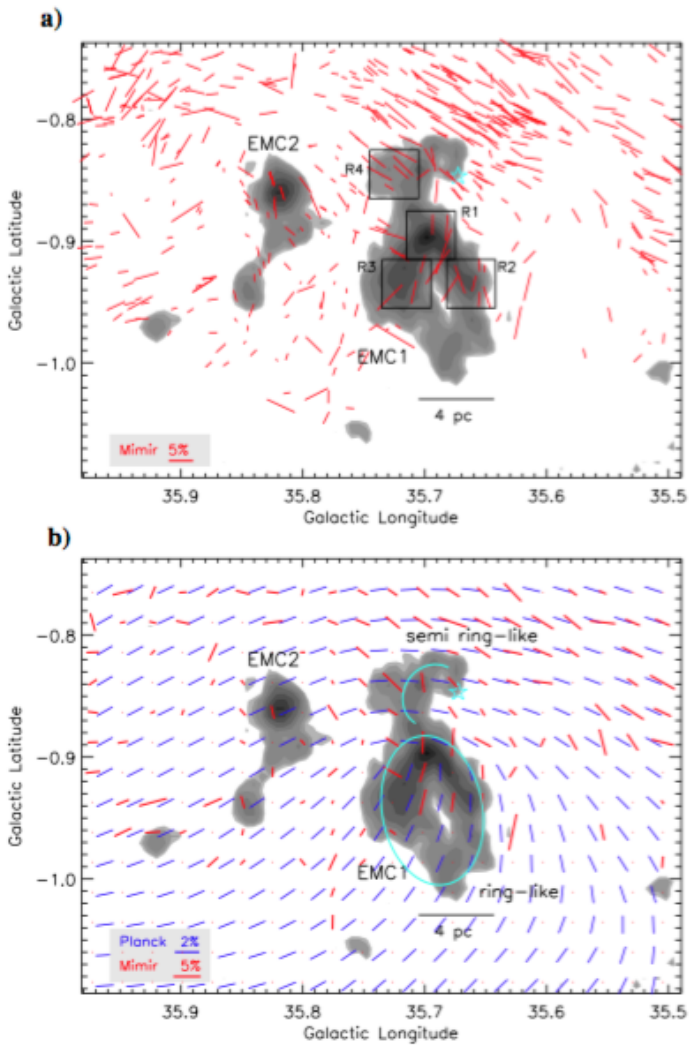

Figure 7. The polarization measurements toward the MCG35.6. a) The GPIPS H-band polarization vectors (in red color) of high quality background stars are drawn on the molecular intensity map. These stars are selected using the criteria $P/\sigma_P \geq 2$, $\sigma_P \leq 5$, $H \leq 13$ and $J - H > 1$. The four subregions targeting the dense clumps/cores are marked by square boxes. The length of each vector shows the degree of polarization. The orientation of each vector shows the Galactic position angle of polarization. b) The *Planck* polarization vectors (in blue) from the dust emission at 353 GHz are overlaid on the molecular intensity map. The vectors are rotated by 90° to infer the POS magnetic field directions. The mean GPIPS polarization vectors (in red) are also overplotted on the molecular map and are obtained by spatially averaging the values matching the same pixel scale of the *Planck* data. In both the panels, the background map is similar to the one shown in Figure 5a. In each panel, a reference vector in the lower left corner is also shown for comparison.

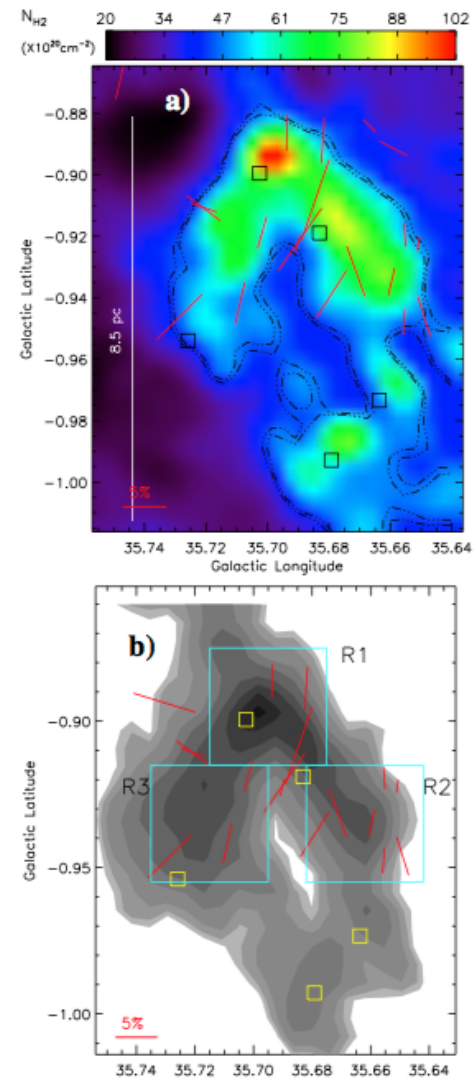

Figure 8. The H-band polarimetric measurements toward the ring-like feature (see Table 3). a) Overlay of GPIPS H-band polarization vectors (in red color) of high quality background stars on the *Herschel* column density map. Column density contours are also shown with levels of [4.5, 4.67] × 10^{21} cm^{-2}. b) Overlay of GPIPS H-band polarization vectors (in red color) of high quality background stars on the integrated ^{13}CO emission map. Three subregions (i.e. R1, R2, and R3) targeting the areas of high column density are marked in big square boxes. A reference vector is also shown in each panel. In both the panels, the *Herschel* clumps are also marked by small squares. At least five clumps appear to be distributed in an almost regularly spaced manner along the ring-like feature.

7. The lithium-rotation connection in the 125 Myr-old Pleiades cluster

J. Bouvier et al. Accepted by A&A https://arxiv.org/pdf/1712.06525.pdf

Context. The evolution of lithium abundance over a star's lifetime is indicative of transport processes operating in the stellar interior.
Aims. We revisit the relationship between lithium content and rotation rate previously reported for cool dwarfs in the Pleiades cluster.
Methods. We derive new LiI 670.8 nm equivalent width measurements from high-resolution spectra obtained for low-mass Pleiades members. We combine these new measurements with previously published ones, and use the Kepler/K2 rotational periods recently derived for Pleiades cool dwarfs to investigate the lithium-rotation connection in this 125 Myr-old cluster.
Results. The new data confirm the correlation between lithium equivalent width and stellar spin rate for a sample of 51 early K-type members of the cluster, where fast rotating stars are systematically lithium-rich compared to slowly rotating ones. The correlation is valid for *all* stars over the (J-K_s) color range 0.50-0.70 mag, corresponding to a mass range from about 0.75 to 0.90 $M_\odot$, and may extend down to lower masses.
Conclusions. We argue that the dispersion in lithium equivalent widths observed for cool dwarfs in the Pleiades cluster reflects an intrinsic scatter in lithium abundances, and suggest that the physical origin of the lithium dispersion pattern is to be found in the pre-main sequence rotational history of solar-type stars.

Key words. Stars: abundances – Stars: low-mass – Stars: rotation – open clusters and associations: individual: Melotte 22 (Pleiades)

8. The dense cores and filamentary structure of the molecular cloud in Corona Australis. Hershel SPIRE and PACS observation from the Herschel Gould Belt Survey

D. Bresnahan et al. Accepted by A&A http://arxiv.org/pdf/1801.07805

We present a catalogue of prestellar and starless cores within the Corona Australis molecular cloud using photometric data from the *Herschel* Space Observatory. At a distance of $d \sim 130$ pc, Corona Australis is one of the closest star-forming regions. *Herschel* has taken multi-wavelength data of Corona Australis with both the SPIRE and PACS photometric cameras in a parallel mode with wavelengths in the range 70 μm to 500 μm. A complete sample of starless and prestellar cores and embedded protostars is identified. Other results from the *Herschel* Gould Belt Survey have shown spatial correlation between the distribution of dense cores and the filamentary structure within the molecular clouds. We go further and show correlations between the properties of these cores and their spatial distribution within the clouds, with a particular focus on the mass distribution of the dense cores with respect to their filamentary proximity. We find that only lower-mass starless cores form away from filaments, while all of the higher-mass prestellar cores form in close proximity to, or directly on the filamentary structure. This result supports the paradigm that prestellar cores mostly form on filaments. We analyse the mass distribution across the molecular cloud, finding evidence that the region around the Coronet appears to be at a more dynamically advanced evolutionary stage to the rest of the clumps within the cloud.

Key words. stars: formation – ISM: clouds – ISM: structure – ISM: individual objects (Corona Australis molecular cloud) – submillimeter

10. Binary energy source of the HH 250 outflow and its circumstellar event

F. Comeron et al. Accepted by A&A https://arxiv.org/pdf/1801.06939

Aims. Herbig-Haro flows are signposts of recent major accretion and outflow episodes. We aim to determine the nature and properties of the little-known outflow source HH 250-IRS, which is embedded in the Aquila clouds.
Methods. We have obtained adaptive optics-assisted *L*-band images with the NACO instrument on the Very Large Telescope (VLT), together with *N*− and *Q*−band imaging with VISIR also on the VLT. Using the SINFONI instrument on the VLT we carried out *H*− and *K*−band integral field spectroscopy of HH 250-IRS, complemented with spectra obtained with the SpeX instrument at the InfraRed Telescope Facility (IRTF) in the *JHKL* bands. Finally, the SubMillimeter Array (SMA) interferometer was used to study the circumstellar environment of HH 250-IRS at 225 and 351 GHz with CO (2-1) and CO (3-2) maps and 0.9 mm and 1.3 mm continuum images.
Results. The HH 250-IRS source is resolved into a binary with 0.″53 separation, corresponding to 120 AU at the adopted distance of 225 pc. The individual components show heavily veiled spectra with weak CO absorption indicative of late-type stars. Both are Class I sources, but their spectral energy distributions between 1.5 μm and 19 μm differ markedly and suggest the existence of a large cavity around one of the components. The millimeter interferometric observations indicate that the gas mainly traces a circumbinary envelope or disk, while the dust emission is dominated by one of the circumstellar envelopes.
Conclusions. HH 250 IRS is a new addition to the handful of multiple systems where the individual stellar components, the circumstellar disks and a circumbinary disk can be studied in detail, and a rare case among those systems in which a Herbig-Haro flow is present.

Key words. stars: binaries; circumstellar matter; winds, outflows; pre-main sequence; individual: IRAS 19190+1048. Interstellar medium: jets and outflows

11. The ionizing source of the bipolar HII region S106: a close massive binary

F. Comeron et al. Accepted by A&A http://arxiv.org/pdf/1801.08958

Context. S106 is one of the best known bipolar HII regions, thoroughly studied and modelled at infrared, submillimeter and millimeter wavelengths, and it is one of the nearest examples of the late stages of massive star formation in which the newly formed star that ionizes it is still surrounded by vast amounts of gas and dust. However, little is known about its heavily obscured central source, S106IR.
Aims. The possible binarity of the central source is investigated, which is considered to be likely given the high binarity fraction among massive stars.
Methods. We have carried out visible and near-infrared photometric monitoring looking for short-term variability, with special interest in that related to the presence of a close binary companion to S106IR that may produce periodic eclipses or tidal distortion of the shape of the members of the system.
Results. A periodic variability of S106IR in the *J* band is found with a period of 5.0 days and an amplitude of $\simeq 0.1$ mag. The light curve displays a slow rise from minimum to maximum followed by a steep decrease, and can be well reproduced by a close binary system composed of two stars with different luminosity orbiting each other in an elliptical orbit of moderate eccentricity. S106IR also shows hints of short-term variability possibly related to accretion. We also report variability of four other stars previously classified as members of the S106 cluster, all of which are strong X-ray emitters.
Conclusions. The newly discovered close binarity of S106IR adds a new element to the modeling of the nebula and to the understanding of the dynamics of the gas around the ionizing source, which suggests that the components of the binary are accreting via a circumbinary disk. Binarity also helps to explain the apparent mismatch between the spectral type of the ionizing source inferred from the nebular spectrum and its high brightness at near-infrared wavelengths.

Key words. Stars: early-type; Binaries: close; ISM: HII regions, photon-dominated regions, S106

13.Rings and gaps in the disc around Elias 24 revealed by ALMA

G. Dipierro et al. Accepted by MNRAS http://arxiv.org/pdf/1801.05812

ABSTRACT

We present Atacama Large Millimeter/sub-millimeter Array (ALMA) Cycle 2 observations of the 1.3 mm dust continuum emission of the protoplanetary disc surrounding the T Tauri star Elias 24 with an angular resolution of $\sim 0.2''$ ($\sim$ 28 au). The dust continuum emission map reveals a dark ring at a radial distance of $0.47''$ ($\sim$ 65 au) from the central star, surrounded by a bright ring at $0.58''$ ($\sim$ 81 au). In the outer disc, the radial intensity profile shows two inflection points at $0.71''$ and $0.87''$ ($\sim$ 99 and 121 au respectively). We perform global three-dimensional smoothed particle hydrodynamic gas/dust simulations of discs hosting a migrating and accreting planet. Combining the dust density maps of small and large grains with three dimensional radiative transfer calculations, we produce synthetic ALMA observations of a variety of disc models in order to reproduce the gap- and ring-like features observed in Elias 24. We find that the dust emission across the disc is consistent with the presence of an embedded planet with a mass of $\sim 0.7\,\mathrm{M_J}$ at an orbital radius of $\sim$ 60 au. Our model suggests that the two inflection points in the radial intensity profile are due to the inward radial motion of large dust grains from the outer disc. The surface brightness map of our disc model provides a reasonable match to the gap- and ring-like structures observed in Elias 24, with an average discrepancy of $\sim$ 5% of the observed fluxes around the gap region.

Key words: protoplanetary discs — planet-disc interactions — dust, extinction